Title

Point-of-use robotic sensors for simultaneous pressure detection and chemical analysis

Journal

Materials Horizons, 6(3)

ISSN

2051-6347

Authors

Amit, Moran

Mishra, Rupesh K

Hoang, Quyen

et al.

Publication Date

2019-03-18

DOI

10.1039/c8mh01412d

Peer reviewed

Materials Horizons

COMMUNICATION

View Article Online
View Journal

Cite this: DOI: 10.1039/c8mh01412d

Received 7th November 2018,
Accepted 20th December 2018

DOI: 10.1039/c8mh01412d

rsc.li/materials-horizons

Point-of-use robotic sensors for simultaneous pressure detection and chemical analysis†

Moran Amit,‡[a] Rupesh K. Mishra,‡[b] Quyen Hoang,[a] Aida Martin Galan,[b] Joseph Wang*[b] and Tse Nga Ng *[a]

The development of sensors for monitoring hazardous materials in security and environmental applications has been increasing in the last few years. In particular, organophosphates pose a serious health threat that affects the food and agriculture industries. Hence, their rapid on-site detection is highly desired, especially through remote robotic sampling that can minimize the exposure of humans to these hazardous chemicals. To handle sample collection, a robotic manipulator requires tactile feedback, to ensure that no damage will be done to either the robot or the other object in contact due to excessive force. To provide tactile feedback, porous polydimethylsiloxane pressure sensors based on a capacitive mechanism were chosen here, and integrated with enzyme-based electrochemical sensors specific for organophosphate compounds (*e.g.* methyl paraoxon). This results in a hybrid physical–chemical sensing glove that can simultaneously measure the pressure and chemical target without interference between the two sensors. Our pressure sensors showed >55% relative capacitance change per 10 kPa applied pressure, with an average sensitivity (*S*) of 0.057 ± 0.004 kPa^{-1} in the 3–20 kPa range and a maximum sensitivity of 0.30 ± 0.08 kPa^{-1} in the <0.05 kPa range. The chemical biosensors showed a detection range of 20–180 μM for methyl paraoxon in the liquid phase. We have thus combined low-cost chemical and pressure sensors together on disposable, retrofitting gloves, and demonstrated simultaneous tactile sensing and organophosphate pesticide detection in a point-of-use robotic field platform that is scalable, economical, and adaptable for different security, environmental, and food-safety applications.

Conceptual insights

There is a pressing need to enable rapid on-site detection of dangerous materials such as organophosphates for security and environmental applications, especially through remote robotic sampling that can minimize the exposure of humans to these hazardous chemicals. A robotic manipulator with tactile feedback is needed to collect samples and to carry out chemical analysis. Such a combination of physical and chemical sensing has not been reported thus far. In this paper, we introduce a novel glove-based sensing system that offers simultaneous real-time monitoring of pressure and chemical signals. The data obtained in this study demonstrate a flexible platform that integrates pressure and chemical sensing and is extendable, as the printed chemical sensor can be easily modified for detecting different analytes. Moreover, the sensors can easily retrofit on existing robots, converting them to economical on-site screening devices for health, environmental, and security applications, where timely chemical information is critical. Such new capabilities would thus bring advanced analytics directly to robotic fingertips.

Introduction

There is an urgent need for sensor technologies that can monitor hazardous materials in a variety of security and environmental applications. In particular, the occurrence of organophosphate (OP) pesticide residues in agricultural products threatens both human and animal health and poses a serious concern in the food and agriculture industries.[1–3] OP compounds are also a security threat as chemical warfare nerve agents.[4] OP pesticides and nerve-agents are highly toxic to the nervous system, and can cause neurological disorders, infertility, fetal birth defects, and even rapid death.[3,4] Rapid on-site detection of OPs in the solid, liquid, and vapor states has been demonstrated using wearable sensor systems.[5–8] However, these examples require a human operator to be put at risk of exposure to hazardous OP compounds. Remote robotic sampling and sensing platforms are needed to avoid placing people in unsafe environments.[9–11] Such safety and security concerns have motivated us to combine physical and chemical sensors that enable robotic manipulators to carry out remote, point-of-use chemical analysis. The novel combination of chemical sensors for screening for OPs and pressure sensing capability allows delegation of the detection mission to robots, providing them with haptic capability to handle arbitrary samples.

[a] Department of Electrical and Computer Engineering, University of California San Diego, La Jolla, CA 92093, USA. E-mail: tnn046@ucsd.edu
[b] Department of Nanoengineering, University of California San Diego, La Jolla, CA 92093, USA. E-mail: josephwang@eng.ucsd.edu

† Electronic supplementary information (ESI) available. See DOI: 10.1039/c8mh01412d
‡ Equal contribution.

Here, we introduce a flexible glove-based sensing system that offers simultaneous real-time monitoring of pressure and chemical signals. The combination of physical and chemical sensing has rarely been reported, and chemical, pressure, and temperature signals are usually monitored separately in health monitoring devices,[12] with the exception of a recent example of an epidermal biomedical electrocardiogram-lactate patch.[13] Temperature measurements have been combined with the reading of different signals, including biochemical or electrophysiological signals, pressure, and/or strain.[14–16] However, there is no demonstration of robotic point-of-use combined pressure–chemical sensing. Our integrated sensors are printed at low cost to be disposable, and hence easy to be stripped off for the purpose of decontaminating robots. The integrated sensors are conformal to retrofitting manipulators for the simultaneous pressure and OP pesticide sensing, to augment surfaces with sensors and extend machine versatilities.

To avoid harming either the robot or the object in contact as a result of uncontrolled force, tactile feedback is desired during the sample collection step. This is especially relevant for scenarios where gentle contact with delicate agriculture produce is essential. To provide tactile feedback, pressure sensors based on piezoelectric, resistive, or capacitive mechanisms are available.[12,17–19] For targeted applications, capacitive pressure sensors are preferred due to the advantages of low sensitivity to temperature and relative humidity changes, low power consumption, high reproducibility, and static pressure detection capability.[18,20,21] The sensitivity of a capacitive sensor is tunable by adjusting the dielectric compressibility; for instance, the sensitivity is increased by choosing softer materials, *i.e.* elastomers with lower elastic moduli, and by designing porous structures[20–25] that further lower elastic moduli from 1 GPa in solid films to around 1–10 MPa in foam dielectrics.[20] Indeed, the sensitivity of porous structures was found to be around 1–2 orders of magnitude higher compared to that of non-porous dielectrics using the same material.[22–25] Porous structures with well-defined patterns usually exhibit higher sensitivity than arbitrary patterns;[12,21,23] however, their fabrication is highly complex. Here, the foam structures of the pressure sensors are easy to fabricate and are optimized by air-to-solid volume ratios for sensitivity and reproducibility to the range of pressures typical for object manipulation in the low (1–10 kPa) and medium (10–30 kPa) pressure regimes.[12,17]

The chemical sensor relies on the reaction of the immobilized enzyme organophosphate hydrolase (OPH, highly specific for OP compounds) and the OP analyte in the solid form.[5] The *p*-nitrophenol product of the OPH reaction is monitored using a three-electrode electrochemical system using square wave voltammetry (SWV) or amperometric techniques. The use of the potential-scanning SWV method further enhances the selectivity of the specific enzymatic reaction towards the field screening of OP threats compared to the fixed-potential amperometric technique.[5,7] On the other hand, the amperometric detection offers promise toward continuous monitoring applications.

In this research, the chemical and pressure sensors are combined together on disposable nitrile polymer gloves, to allow simultaneous tactile sensing and OP pesticide detection in a point-of-use platform, with no interference with each other. While glove substrates are used here, the sensors are flexible and conformal and easily adjustable to other shapes besides glove surfaces, to equip robots to be on-site screening tools for health, environmental, and security applications where timely chemical information is critical.

Results and discussion

The new physical–chemical hybrid glove sensor integrates the monitoring of the chemical threat with that of physical pressure. Such a dual-sensing ''swipe, sense, and alert'' strategy brings an advanced analytics capability directly to the robotic manipulator. The schematic in Fig. 1a shows the dual sensors integrated on a glove for a robotic hand, wherein the pressure sensor is coupled with a circular swiping pad to collect the chemical threat on one digit, while the chemical sensing electrodes are screen printed onto a separate digit. The electrochemical analysis of the collected threat is carried out by placing the three-electrode system in contact with the collection pad, as shown in Fig. 1b, and meanwhile the contact pressure is simultaneously monitored during this step as well to confirm a secure contact. By placing the pressure sensor under the glove with the printed sample collection pad (Fig. 1c), it is possible to combine the mechanical sampling of the chemical threat with simultaneous pressure measurements. A second sensor configuration, where the collection pad is attached directly to the pressure sensor, is also possible. By mounting the pressure sensor under the glove substrate (Fig. 1c), it is isolated from the outward glove surface with contaminants, which makes this configuration preferred. A glass support was used under the pressure sensors to minimize bending effects.[26,27] The schematic in Fig. 1d shows that the two sensors are coordinated using a central laptop, which controls the measurement sequence of the two electronic boards catered to each sensor type. The circuit boards are a potentiostat circuit[7] and a capacitance-to-digital converter (CDC, chip FDC1004EVM from Texas Instruments) that simultaneously record data from the chemical and pressure sensors, respectively.

The pressure detection mechanism is based on a simple parallel plate capacitor model in Fig. 1e with $C = \varepsilon_0\varepsilon_r A/d$, where C is the capacitance, ε_0 is the permittivity of vacuum, ε_r is the relative permittivity of the material, A is the area of the plates, and d is the distance between the plates. The capacitance sensor is made from a porous polydimethylsiloxane (PDMS) dielectric layer that is sandwiched between two conductive flexible electrodes made of a mixture of Ag particles and PDMS. Applying pressure to the porous PDMS dielectric results in a change in d, and hence in the capacitance. Fig. 1f shows a schematic of the electrochemical detection of an OP compound, methyl paraoxon (MPOx), using the enzyme OPH cast on the glove substrate over the working electrode. The electrochemical response of the OPH reaction product *p*-nitrophenol is thus proportional to the concentration of the target pesticide (substrate). The digit with the collection pad is brought into

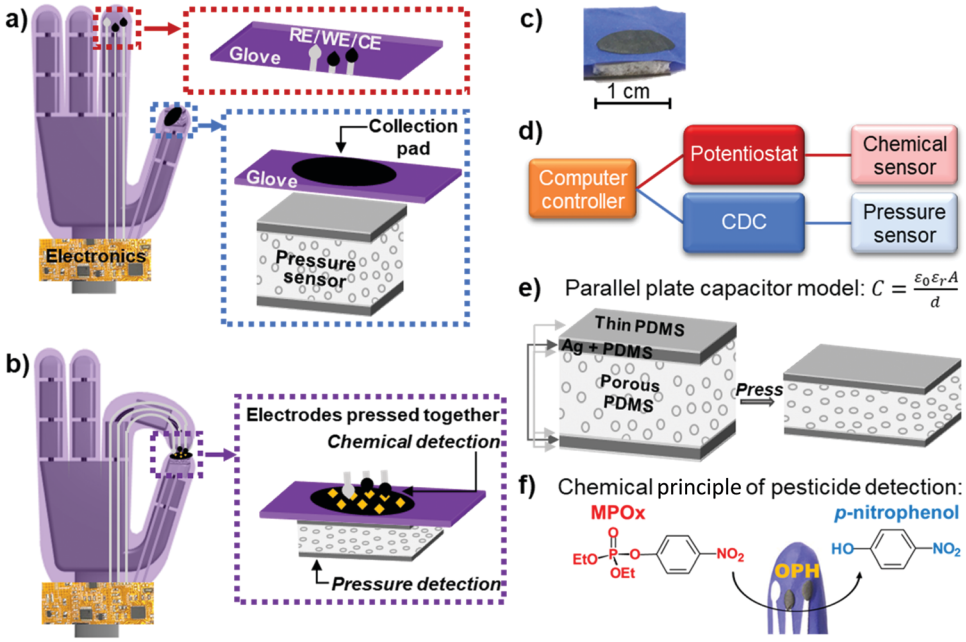

Fig. 1 Dual-functionality glove design and principal operation mechanisms. (a) The glove combines both pressure and chemical sensors. Reference (RE), working (WE), and counter (CE) electrodes are screen printed onto one digit, and the collection pad is printed onto a separate digit. (b) The electrodes are pressed together to initiate the electrochemical analysis. (c) The pressure sensor is below the glove substrate underneath the chemical sensor collection pad. (d) System architecture. (e) The pressure sensor is based on a parallel plate capacitor with a porous PDMS dielectric and flexible electrodes. (f) The chemical sensor detects the reaction product *p*-nitrophenol using three-electrode electrochemical techniques, including SWV and amperometry.

contact with the digit with the three printed electrodes, coated with electrolyte gel, to achieve a complete electrical circuit for performing the SWV and amperometric measurements.

The pressure sensors in this work are porous PDMS capacitors with an area of 1×1 cm^2 and a thickness of 3 mm (Fig. 2a and b). The porous dielectric is easily patterned by mixing different volume proportions of table salt NaCl into uncured PDMS. After curing, the film is submerged in deionized water to leach out all the NaCl, leaving behind air voids in the PDMS dielectric (Fig. 2c). To calibrate the pressure sensors, the capacitance as a function of time was measured under various applied pressures up to $\sim$30 kPa (ESI,† Fig S1). The relative capacitance change $\Delta C/C_0$ as a function of the applied pressure is shown in Fig. 2d, for different volume percentages (vol%) of air in the sensor. The $\Delta C/C_0$ value increases as the volume percentage of pores is changed from 41% to 85%. However, for a porosity value of 90 vol%, the structure was not mechanically robust, with collapsed air voids that reduced compressibility. Hence, the most sensitive capacitor is the 85 vol% PDMS foam that reached $>$55% relative capacitance change per 10 kPa pressure. The sensitivity of these sensors, typically defined as the slope of $\Delta C/C_0$ as a function of the pressure, was $S = 0.057 \pm 0.004$ kPa^{-1} in the 3–20 kPa range (Fig. 2e and Fig. S2, ESI‡). This is 3–5 fold higher than those of other unpatterned porous elastomeric structures in a similar pressure regime,[22,24,25] and with a higher operating range compared to a different PDMS foam structure that exhibited similar relative capacitance change.[21]

While the $\Delta C/C_0$ per 10 kPa pressure value of our pressure sensor is 3–4 fold lower than that of photolithographically patterned porous PDMS sensors, its fabrication process is much simpler.[23] In addition, the highest sensitivity of the 85 vol% PDMS foam sensors that was measured to be 0.30 ± 0.08 kPa^{-1} in the very low pressure regime $<$0.05 kPa (Fig. S2, ESI‡) is in the same order of magnitude as state-of-the-art porous PDMS sensors.[23] There is a transition in the slope around 10 kPa for the 41, 80, and 90 vol% porosity sensors (Fig. 2d), when the compressibility of the dielectric starts to saturate. For the 85 vol% PDMS porous sensors such transition is not noticeable. Effectively, such slope change enables the detection of higher pressures. The capacitors with 80 and 85 vol% air were pressed for 50 cycles and showed no significant change in performance, demonstrating the stability of the pressure sensors (Fig. 2e and Fig. S3, ESI‡). The calibration curves for 10 different pressure sensors are shown in Fig. S4 (ESI‡), demonstrating sensor reproducibility, and we note that this approach is easy and scalable for modeling porous structures over large areas.

The chemical sensors were individually calibrated with analytes in the liquid phase, as shown in Fig. 3a and Fig. S5 (ESI‡). The performance of the sensor towards the electrochemical detection of the OP compound MPOx was evaluated in a 0.1 M phosphate buffer solution containing increasing (20–200 μM) MPOx concentrations. A background scan was recorded before performing the liquid phase tests. Upon biosensing MPOx by the OPH biocatalytic reaction, an anodic signal appeared due to the oxidation of the *p*-nitrophenol product, which is proportional to the level of the hydrolyzed MPOx. For measurement, a SWV was performed in the potential range between 0.3 and 1.0 V. The voltammograms show a defined oxidation peak at +0.7 V in liquid samples and displays sensitivity towards micromolar MPOx concentrations. The lower

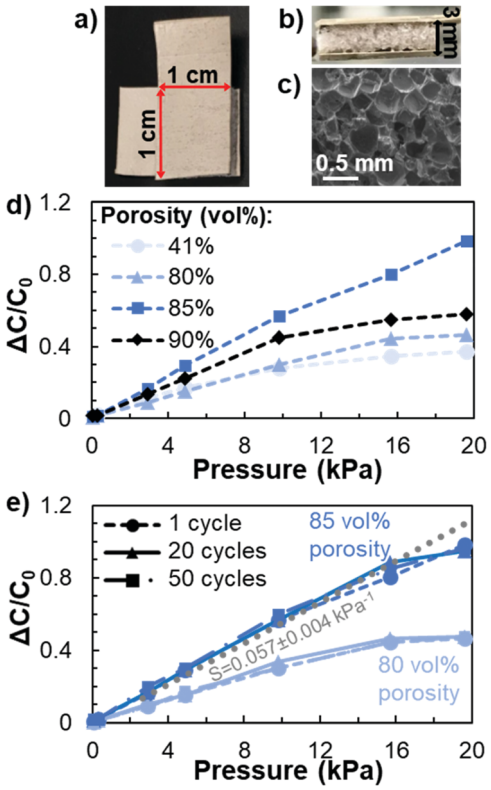

Fig. 2 Pressure sensor characteristics. (a) Top and (b) side views of the capacitive pressure sensor. (c) SEM micrograph of the porous dielectric. (d) Relative capacitance change as a function of the applied pressure. The porosity legend indicates the volume percentage of air in the sensor. (e) Reproducibility of the pressure sensor's response under repeated cycles of the applied pressure. The initial capacitances of all fabricated sensors are around 4–8 pF. The gray notation marks the sensitivity of the 85 vol% porosity sensors.

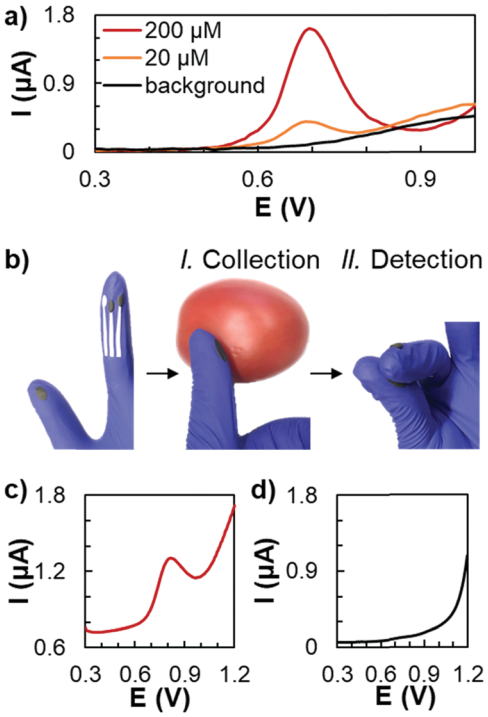

Fig. 3 Chemical sensor characteristics. (a) Square wave voltammograms at different MPOx concentrations in 0.1 M phosphate buffer solutions, with the background current subtracted from the signals. The SWV potential range is 0.3–1.0 V *vs.* Ag/AgCl using a frequency of 10 Hz and an amplitude of 25 mV. (b) Operational steps for pesticide detection: (I) a collection pad is used to swipe the surface containing the pesticide and (II) the collection pad and electrodes are pressed together to allow chemical analysis. For clarity, the electrical wires between the electrodes and the readout boards are omitted in this photo. (c and d) Screening of the MPOx pesticide on the surface of a tomato for food safety assessment. SWVs of the tomato contaminated with the MPOx pesticide and of the non-spiked control sample, respectively. SWV conditions for parts c and d: the voltage range is +0.3 to +1.2 V *vs.* Ag/AgCl, at a frequency of 10 Hz and an amplitude of 25 mV.

limit of detection in the liquid phase reaches down to 20 μM, as shown in Fig. S3 (ESI‡), with the response increasing linearly up to 180 μM before it reaches saturation. According to the National Institute for Occupational Safety and Health in the US, cytogenetic effects and DNA damage to human sperm were found for ~300 μM h^{-1}. The detection limit of our OP sensor is thus sufficient for monitoring toxicity levels relevant to human health.

Subsequently for trace solid detection, Fig. 3b displays the typical procedure for point-of-use pesticide screening, such as that on the surface of a tomato sample. Such solid detection relies on the mechanical accumulation of the OP sample residues. The model MPOx pesticide was thus used to contaminate the tomato surface using 200 μL solution at 200 μM concentration, in comparison with a control surface (a tomato without MPOx). After the solution evaporated and the tomato surface was dried, the first step was to swipe the sample surface using the manipulator digit containing the carbon collection pad. Then, to initiate electrochemical measurements, the collector pad was pressed against the measurement electrodes to complete the electrochemical cell, and signal generation was based on the biocatalytic activity of the immobilized OPH enzyme. Note that during this step the pressure was also measured, as will be illustrated in the following sections. Fig. 3c reveals a clear voltammetric detection of MPOx on the contaminated tomato. The distinct SWV peak at around +0.80 V, associated with the nitrophenol product, shows an efficacious detection by the printed chemical sensor for screening tests. Notice the small shift in the peak potential of the dry test compared to the liquid-phase measurements (Fig. 3a) that reflects the nature of the dry test (and the corresponding electrolyte-gel coating). Fig. 3d illustrates the response of the non-spiked control sample, wherein a flat baseline curve was obtained without any voltammetric signature of the phenolic product.

The key to remote robotic measurements was the coordination of touch and chemical sensing procedures. Fig. 4 shows simultaneous monitoring of pressure and chemical signals. The readings from the pressure sensor indicated that the manipulator's collection pad was in good contact with the sample surface during the collection step (yellow region). Subsequently, the collection pad was brought into contact with the measurement electrodes during the chemical detection step

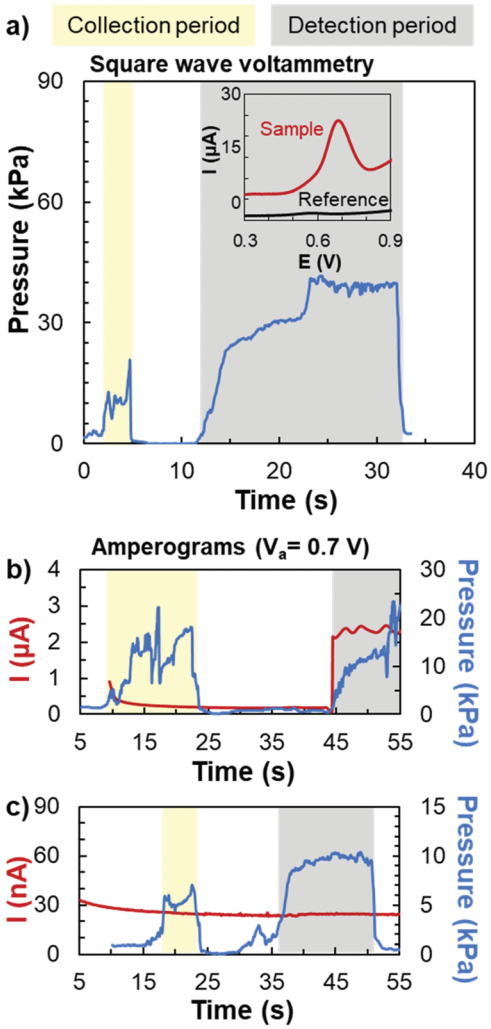

Fig. 4 Simultaneous pressure and chemical detection. (a) Pressure sensor measurements during the sample collection step (yellow region) and the chemical detection step (gray region). The electrochemical SWV scans in the inset were initiated when the collection pad was pressed and in good contact with the measurement electrodes, as indicated by the exceeding pressure. The same color schemes are used for collection and detection periods for plots b and c. Simultaneous measurements of pressure and amperograms at an applied potential of +0.7 V. The electrochemical sensor current increased for (b) the tomato sample spiked with MPOx (200 μL at 200 μM concentration). The current did not change for (c) the control tomato surface with no pesticide, while the pressure signal indicated that the collection pad and measurement electrodes are in good contact for proper electrical connections during the electrochemical measurements.

(gray region). There is negligible difference in the pressure sensor capacitance (less than 0.1 pF change in capacitors of 4–8 pF; namely, less than 2% change) before and after the analyte collection. In Fig. 4a, the electrochemical SWV scans in the inset were initiated when the collection pad was pressed and in good contact with the measurement electrodes, as evidenced by the exceeding pressure. The peak observed in the SWV measurement showed positive detection of MPOx on the contaminated tomato sample.

In addition to SWV, another electrochemical detection approach was to measure amperograms at a fixed potential, corresponding to the oxidation of the nitrophenol enzymatic reaction product. Thus, in Fig. 4b and c the electrochemical sensor current was continuously monitored at +0.7 V. Meanwhile, the pressure signals indicated that the manipulator was pressed onto the sample during the collection phase so that the collection pad and measurement electrodes were in good contact for proper electrical connections during electrochemical measurements. We observe that with a low pressure of $\sim$2 kPa, the chemical reaction already took place. The detection of solid analytes is qualitative to determine the presence or absence of MPOx. The current response of the electrochemical sensor increased for the tomato sample spiked with MPOx, as shown in Fig. 4b. The current slightly faded with time because the reaction product was consumed. As a control confirmation, no current change was observed for the tomato with no pesticide, as shown in Fig. 4c. Overall, Fig. 4 shows that pressure and chemical signals can be measured simultaneously with no interference between them.

Conclusions

We described a robotic retrofitting device that can simultaneously measure the chemical target and pressure using the same glove form factor. Our integrated glove incorporated pressure and chemical sensors to coordinate a point-of-use procedure for robotic manipulators to carry out remote detection of an organophosphate pesticide, methyl paraoxon. By combining haptic capability and chemical sensing functionality, the sensor glove increases the range of missions that robots can perform. A similar 'swipe and detect' dual-sensing procedure could benefit the remote detection of other hazardous materials, particularly explosive residues. The printed flexible sensors are economical for augmenting machine surfaces with sensing capabilities. While a glove form factor was demonstrated here, the sensors could be used to retrofit conformally on other shapes.

Here, the capacitive pressure sensors showed more than 55% relative capacitance change per 10 kPa pressure, with a sensitivity (S) of 0.057 $\pm$ 0.004 kPa^{-1} in the 3–20 kPa range and a maximum sensitivity of 0.30 $\pm$ 0.08 kPa^{-1} in the subtle-pressure regime $<$0.05 kPa. The operation range tested was up to $\sim$30 kPa, yet the sensors show no saturation at this point; hence, their operation range could be extended even further with proper calibration. The electrochemical sensors displayed a lower detection limit of 20 μM MPOx in the liquid phase and reached saturation at 180 μM MPOx. This point-of-use robotic glove could be used as the frontline protection of OP threat and pesticide screening, avoiding human exposure to contaminated produce. The promising data obtained in this study supports the possibility of developing advanced flexible, retrofitting sensors that integrate multiple chemical and physical sensors on the same platform. The platform is extendable in terms of increasing the numbers and types of chemical sensors to other applications, as the printed chemical sensor can be easily modified not only for detecting different analytes in agricultural applications, but also for detecting security and

environmental hazards. Such new capabilities would thus bring advanced analytics directly to ''robotic fingertips''.

Methods

Chemicals and reagents

Purple nitrile powder-free exam gloves (Kimberly-Clark, Roswell, GA), carbon ink (E3449, Ercon, Inc., Wareham, MA) and Ag/AgCl ink (E2414, Ercon, Inc., MA), potassium ferricyanide, dipotassium hydrogen phosphate (K_2HPO_4), potassium dihydrogen phosphate (KH_2PO_4), methyl paraoxon, Nafion, agarose and ethanol were purchased from Sigma-Aldrich. All purchased chemicals were of analytical standard grade and were used without further purification. Ultrapure deionized water was used in the preparation of aqueous electrolyte solutions. Polydimethylsiloxane (PDMS) base and a curing agent (Sylgard 184, Dow Corning), sodium chloride (NaCl, Fisher Chemical), and conductive epoxy (CW2400, Chemtronics) were used for pressure sensor fabrication. Tomatoes were purchased from local shops of San Diego, CA. The OPH enzyme (10 μg mL^{-1}) was isolated from *E. coli* bacterial strain DH5α. The isolation, expression, purification, and crystallization were performed following the procedure described elsewhere.[28] The OPH enzyme stability in Nafion was evaluated for several days with a stable electrochemical response observed for one week, after which the response decreases gradually.

Pressure sensor fabrication

To prepare a PDMS foam dielectric, the curing agent was mixed with PDMS base in a 1 : 10 weight ratio. The PDMS mixture was then thoroughly mixed with NaCl. To achieve different volume percentages of porosity[25] for this study, the NaCl to PDMS volume ratio was adjusted accordingly. The mixture was placed into a Petri dish and pressed to a desired thickness prior to curing it on a hot plate at 90 °C for about 90 minutes. After curing, the material was placed into a large beaker with deionized water to leach out all the NaCl, leaving behind air voids in the PDMS. Water was changed several times over a 24–48 h period to ensure that all the NaCl had been leached out. The remaining PDMS foam was then air-dried and cut into 1×1 cm^2 pieces prior to the attachment of electrodes.

To fabricate flexible Ag electrodes, the PDMS mixture was cast in a rectangular mold that was roughly 400 μm deep, prior to curing it on a hot plate at 90 °C for 1 h, to form the outermost encapsulation layer. The mold base was a glass slide, while its walls consisted of 3 stacking layers of duct tape. For the conductive layer of the electrodes a flexible conductive layer was made of a mixture of Ag particles and an elastomer.[29,30] In particular, Ag/AgCl ink was mixed thoroughly with the PDMS mixture, at weight percentages of 12.5% and 87.5%, respectively. PDMS was used in this mixture to enhance the flexibility of the cured silver electrode and improve adhesion to the dielectric, while a high content of Ag reduced the electrical resistance of the electrode to $\sim 0.5\ \Omega$.[31] The conductive mixture was deposited on the pre-made PDMS encapsulation layer *via* a doctor blade and cured at 100 °C for 1 h. After curing, a small area of the conductive electrode was blade coated with a very thin layer of the PDMS mixture, which functioned as a 'glue' layer between the PDMS foam dielectric and the electrode. PDMS foam pieces each with an area of 1×1 cm^2 were placed on the uncured PDMS and cured at 90 °C for 30 min. The attachment process was repeated for the second sensor electrode. The exposed areas of the electrode were connected to thin electrical wires using conductive epoxy, and then covered with a PDMS layer followed by curing at 90 °C for 30 min for protection. The thin electrical wires connected the sensor to a capacitance-to-digital converter (CDC) board.

Pressure sensor calibration and pressure detection

For the calibration of each pressure sensor, the capacitor was connected to a CDC board (FDC1004EVM, Texas Instruments Incorporated) or to an LCR meter (E4980AL, Keysight). The initial capacitance C_0 was measured without an applied pressure. Then different known weights in ascending order were placed on a plastic holder on top of the capacitor, which was placed on a solid surface, and the corresponding capacitance to each weight was recorded (Fig. S1, ESI‡). The plastic holder served two purposes: (1) to eliminate the interference between the metal weights and the capacitor and (2) to ensure a constant contact area. The corresponding pressure P to each weight was calculated using the equation $P = F/A = mg/A$, where F is the applied force, m is the known mass of the placed weight, $g = 9.81$ m s^{-2} is the gravitational constant, and A is the contact area onto which the pressure was applied. The calibration curve $\Delta C = C - C_0$ *vs.* P allowed conversion of the measured capacitance to pressure.

Chemical sensor fabrication

The Ercon carbon and Ag/AgCl inks were used for screen printing of the sensors onto gloves.[30] The fabrication utilized a semiautomatic MPM-SPM screen printer (Speedline Technologies, Franklin, MA). The mask for the sensor printing was designed using AutoCAD (Autodesk, San Rafael, CA) and purchased as stainless steel through-hole 12″ × 12″ framed stencils of 125 μm thickness (Metal Etch Services, San Marcos, CA). The finger design planar glove molds ($10.0 \times 2.3 \times 1.3$ cm^3 dimensions) were designed using SolidWorks 3D CAD (DS SolidWorks, Waltham, MA) and produced using a Mojo 3D printer (Stratasys, Eden Prairie, MN). The 3D printed finger design molds were inserted into the purple nitrile gloves, to enable a planar printing surface, immediately before screen-printing the sensor structures. The printing method of the electrodes involved a 125 μm thick layer sequence of (a) Ag/AgCl ink, (b) carbon ink from Ercon and (c) a protecting insulator layer composed of flexible, stretchable adhesive (Aleene's, Inc., Fresno, CA). The Ag/AgCl-ink was used for the reference electrode, whereas the carbon ink was used for working and counter electrode printing. The insulating layer was printed onto the Ag/AgCl interconnects to offer a dielectric separation of the three-electrode system and avoids device short-circuits. For the collection pad, a circular carbon ink based pad disk was printed. The screen-printed sensor electrode patterns were cured at 70 °C for 10 min after each layer was printed.

Prior to the OPH enzyme immobilization, the sensor surface was cleaned by applying cyclic voltammetry (CV) in the range 0.2 to +1.0 V using 0.01 M sodium acetate buffer (pH 4.5) with a scan rate of 0.1 V s^{-1} for 20 cycles. Later, the enzymatic bioreagent layer was fabricated by coating the working electrode with a mixed Nafion/OPH layer. This was accomplished by first preparing a solution of 1% Nafion in ethanol, and a separate solution of OPH enzyme (20 μg mL^{-1}) in 0.1 M phosphate buffer (pH 7.4). The Nafion and OPH solutions were then mixed (500 μL) at a 7 : 3 v/v ratio and a 5 μL aliquot of this mixture was drop-cast onto the clean working electrode surface (on the index finger). The electrode was allowed to dry at room temperature for at least 3 h.

Pesticide detection using a glove biosensor

MPOx was first detected in the liquid phase to assess the performance of the fabricated glove biosensors. The analyses of OPs in the liquid and dry phases were carried out inside the fume-hood following firm safety measures. Experiments were conducted by varying the MPOx concentrations from 20 to 200 μM in the liquid phase. SWVs were recorded at room temperature (22 °C) using the enzyme-modified carbon electrode as the working electrode through the electronic board attached to the glove. These voltammograms were recorded using an electrochemical analyzer (CHI 1232A, CH Instruments, Austin, TX) controlled by MATLAB through a measuring interface between the +0.3 V and +1.2 V potential range using a SWV frequency of 10 Hz, an amplitude of 25 mV, and a 4 mV step.

For detection in the solid phase, a food sample tomato surface was first wiped with 70% ethanol, then distilled water and dried. Subsequently, the tomato surface was contaminated using OP compound methyl paraoxon (200 μM in 5% v/v acetonitrile). A 200 μL aliquot of MPOx was cast on the surface of the tomato, and the aliquot was allowed to dry to a residue through evaporation at room temperature. The tomato surface was rubbed using the digit with the collection pad to mechanically collect analyte residues onto the printed carbon disk. A conductive semisolid agarose gel matrix was used to complete the electrochemical cell by following a previous paper.[5] In brief, a mixture of 0.5 wt% agarose in a 100 mM KCl and 100 mM KH_2PO_4 buffer was heated in a small glass vial at 100 °C for 15 min (600 rpm, until homogenized). The solution was then added to the sensor surface to solidify. The digit with the collected analyte residues was brought into contact with the other digit containing the conductive electrolyte gel to achieve a complete electrical circuit essential for performing the electrochemical measurements. Each glove was used for one-time analysis carried out in the fume-hood for safety.

Positioning the sensors

The chemical sensor was printed onto a nitrile glove as discussed above, and the pressure sensor was placed on a rigid glass support to minimize bending effects and inserted under the printed collection pad prior to using the glove, so it is underneath the glove away from contaminants and potentially can be re-used.

Safety note

Due to the extremely toxic nature of OP compounds, experiments were conducted by following strict safety measures, wearing safety goggles and a respiratory mask.

Conflicts of interest

There are no conflicts to declare.

Acknowledgements

The authors would like to thank the UCSD Center for Wearable Sensors for funding support. M. A. was supported by the Postdoctoral Fellowship for Women Scientists from the Planning and Budgeting Committee, the Council for Higher Education, Israel. This work was supported by the Defense Threat Reduction Agency Joint Science and Technology Office for Chemical and Biological Defense (HDTRA 1-16-1-0013).

References

1 B. Eskenazi, A. Bradman and R. Castorina, Exposures of children to organophosphate pesticides and their potential adverse health effects, *Environ. Health Perspect.*, 1999, **107**, 409.
2 M. Jokanovic and M. Kosanovic, Neurotoxic effects in patients poisoned with organophosphorus pesticides, *Environ. Toxicol. Pharmacol.*, 2010, **29**, 195.
3 S. Chowdhary, R. Bhattacharyya and D. Banerjee, Acute organophosphorus poisoning, *Clin. Chim. Acta*, 2014, **431**, 66.
4 J. Bajgar, Organophosphates/nerve agent poisoning: Mechanism of action, diagnosis, prophylaxis, and treatment, *Adv. Clin. Chem.*, 2004, **38**, 151.
5 R. K. Mishra, L. J. Hubble, A. Martin, R. Kumar, A. Barfidokht, J. Y. Kim, M. M. Musameh, I. L. Kyratzis and J. Wang, Wearable Flexible and Stretchable Glove Biosensor for On-Site Detection of Organophosphorus Chemical Threats, *ACS Sens.*, 2017, **2**, 553.
6 J. R. Sempionatto, R. K. Mishra, A. Martin, G. D. Tang, T. Nakagawa, X. L. Lu, A. S. Campbell, K. M. J. Lyu and J. Wang, Wearable Ring-Based Sensing Platform for Detecting Chemical Threats, *ACS Sens.*, 2017, **2**, 1531.
7 R. K. Mishra, A. Martin, T. Nakagawa, A. Barfidokht, X. L. Lu, J. R. Sempionatto, K. M. Lyu, A. Karajic, M. M. Musameh, I. L. Kyratzis and J. Wang, Detection of vapor-phase organophosphate threats using wearable conformable integrated epidermal and textile wireless biosensor systems, *Biosens. Bioelectron.*, 2018, **101**, 227.
8 R. K. Mishra, A. Barfidokht, A. Karajic, J. R. Sempionatto, J. Wang and J. Wang, Wearable potentiometric tattoo biosensor for on-body detection of G-type nerve agents simulants, *Sens. Actuators, B*, 2018, **273**, 966.
9 H. Ishida, Y. Wada and H. Matsukura, Chemical Sensing in Robotic Applications: A Review, *IEEE Sens. J.*, 2012, **12**, 3163.
10 T. F. Lu, Indoor odour source localisation using robot: Initial location and surge distance matter?, *Robot. Auton. Syst.*, 2013, **61**, 637.

11 M. Turduev, G. Cabrita, M. Kirtay, V. Gazi and L. Marques, Experimental studies on chemical concentration map building by a multi-robot system using bio-inspired algorithms, *Auton. Agents Multi Agent Syst.*, 2014, **28**, 72.
12 Y. H. Lee, O. Y. Kweon, H. Kim, J. H. Yoo, S. G. Han and J. H. Oh, Recent advances in organic sensors for health self-monitoring systems, *J. Mater. Chem. C*, 2018, **6**, 8569.
13 S. Imani, A. J. Bandodkar, A. M. V. Mohan, R. Kumar, S. F. Yu, J. Wang and P. P. Mercier, A wearable chemical-electrophysiological hybrid biosensing system for real-time health and fitness monitoring, *Nat. Commun.*, 2016, **7**, 11650.
14 W. Gao, S. Emaminejad, H. Y. Y. Nyein, S. Challa, K. V. Chen, A. Peck, H. M. Fahad, H. Ota, H. Shiraki, D. Kiriya, D. H. Lien, G. A. Brooks, R. W. Davis and A. Javey, Fully integrated wearable sensor arrays for multiplexed in situ perspiration analysis, *Nature*, 2016, **529**, 509.
15 T. Q. Trung, S. Ramasundaram, B.-U. Hwang and N.-E. Lee, An All-Elastomeric Transparent and Stretchable Temperature Sensor for Body-Attachable Wearable Electronics, *Adv. Mater.*, 2016, **28**, 502.
16 W.-H. Yeo, Y.-S. Kim, J. Lee, A. Ameen, L. Shi, M. Li, S. Wang, R. Ma, S. H. Jin, Z. Kang, Y. Huang and J. A. Rogers, Multifunctional Epidermal Electronics Printed Directly Onto the Skin, *Adv. Mater.*, 2013, **25**, 2773.
17 Y. Zang, F. Zhang, C.-A. Di and D. Zhu, Advances of flexible pressure sensors toward artificial intelligence and health care applications, *Mater. Horiz.*, 2015, **2**, 140.
18 T. T. Yang, D. Xie, Z. H. Li and H. W. Zhu, Recent advances in wearable tactile sensors: Materials, sensing mechanisms, and device performance, *Mater. Sci. Eng., R*, 2017, **115**, 1.
19 Y. B. Wan, Y. Wang and C. F. Guo, Recent progresses on flexible tactile sensors, *Mater. Today Phys.*, 2017, **1**, 61.
20 C. Metzger, E. Fleisch, J. Meyer, M. Dansachmuller, I. Graz, M. Kaltenbrunner, C. Keplinger, R. Schwodiauer and S. Bauer, Flexible-foam-based capacitive sensor arrays for object detection at low cost, *Appl. Phys. Lett.*, 2008, **92**, 013506.
21 B. Y. Lee, J. Kim, H. Kim, C. Kim and S. D. Lee, Low-cost flexible pressure sensor based on dielectric elastomer film with micro-pores, *Sens. Actuators, A*, 2016, **240**, 103.
22 S. Chen, B. Zhuo and X. Guo, Large Area One-Step Facile Processing of Microstructured Elastomeric Dielectric Film for High Sensitivity and Durable Sensing over Wide Pressure Range, *ACS Appl. Mater. Interfaces*, 2016, **8**, 20364.
23 S. Kang, J. Lee, S. Lee, S. Kim, J. K. Kim, H. Algadi, S. Al-Sayari, D. E. Kim, D. Kim and T. Lee, Highly Sensitive Pressure Sensor Based on Bioinspired Porous Structure for Real-Time Tactile Sensing, *Adv. Electron. Mater.*, 2016, **2**, 1600356.
24 O. Atalay, A. Atalay, J. Gafford and C. Walsh, A Highly Sensitive Capacitive-Based Soft Pressure Sensor Based on a Conductive Fabric and a Microporous Dielectric Layer, *Adv. Mater. Technol.*, 2018, **3**, 1700237.
25 Y. Zhai, J. Lee, Q. Hoang, D. Sievenpipper, H. Garudadri and T. N. Ng, A printed wireless fluidic pressure sensor, *Flexible Printed Electron.*, 2018, **3**, 035006.
26 S. Lee, A. Reuveny, J. Reeder, S. Lee, H. Jin, Q. Liu, T. Yokota, T. Sekitani, T. Isoyama, Y. Abe, Z. Suo and T. Someya, A transparent bending-insensitive pressure sensor, *Nat. Nanotechnol.*, 2016, **11**, 472.
27 C. M. Boutry, M. Negre, M. Jorda, O. Vardoulis, A. Chortos, O. Khatib and Z. Bao, A hierarchically patterned, bioinspired e-skin able to detect the direction of applied pressure for robotics, *Sci. Rob.*, 2018, **3**, eaau6914.
28 H. Yang, P. D. Carr, S. Y. McLoughlin, J. W. Liu, I. Horne, X. Qiu, C. M. J. Jeffries, R. J. Russell, J. G. Oakeshott and D. L. Ollis, Evolution of an organophosphate-degrading enzyme: a comparison of natural and directed evolution, *Protein Eng.*, 2003, **16**, 135.
29 K. P. Wang, U. Parekh, T. Pailla, H. Garudadri, V. Gilja and T. N. Ng, Stretchable Dry Electrodes with Concentric Ring Geometry for Enhancing Spatial Resolution in Electrophysiology, *Adv. Healthcare Mater.*, 2017, **6**, 1700552.
30 S. Ready, F. Endicott, G. L. Whiting, T. N. Ng, E. M. Chow and J. P. Lu, *3D Printed Electronics*, NIP & Digital Fabrication Conference, 2013, vol. 1, p. 9.
31 A. J. Bandodkar, R. Nuñez-Flores, W. Jia and J. Wang, All-Printed Stretchable Electrochemical Devices, *Adv. Mater.*, 2015, **27**, 3060.

